Supplementary materials

Additional Methods

Haplotype structure comparison using Haplostrips

We used the software *Haplostrips* (Marnetto and Huerta-Sánchez 2017) to plot the haplotypes from the *Chr11Max* region from the simulations. The haplotype input matrix for the software was generated from SLiM (Haller and Messer 2018) by the end of one replicate of simulation, and was further truncated to include only the center 100kb region surrounding the exon where the beneficial mutation arises when applicable. We sampled 100 chromosomes from the donor, recipient, and the outgroup populations respectively. The software output displayed each variant within the region as a column, and each row represents a haplotype (phased from the simulation; Figure S3). Each population was assigned a unique color corresponding to the haplotypes from the respective population. The haplotypes were hierarchically clustered in two ways: 1) sorted and clustered by a decrease in similarity to the sampled haplotypes from the donor population (Figure S3A); 2) clustered by population first, and sorted by a decrease in similarity to the donor population (Figure S3B). The panels on the right-hand side in Figure S3A represent the distribution of haplotypes in terms of the genetic distance to the donor haplotypes.

Alternate models of selection in modern humans

We explored how the dominance coefficient (h) affects the FPRs in regions including the *HLA* and *HYAL2 genes*. We simulated these regions under the deleterious model using Model_h demography, but with the dominance coefficient for the deleterious mutations varying between being complete recessive (h=0) to additive (h=0.5). We additionally employed a dominance model for humans where h depends on the strength of negative selection (hs relationship (Henn *et al.* 2016)). For each of the dominance value, we obtained 100 replicates.

To explore whether the time of positive selection affects the distribution of AI statistics on *HLA* and *HYAL2*, we performed additional simulations of these regions using the selection on "Standing Archaic Variation" (SAV) scenario (Jagoda *et al.* 2017) under the modern human demography (Model_h), which in effect resembles a type of weaker positive selection. In the SAV simulations, upon entering the recipient population, the adaptively introgressed mutation is neutral for the first 500 generations before it resumes its beneficial fitness effect. The simulations are performed using the realistic recombination map and genomic structure of the respective gene regions, and are repeated for 100 replicates per region.

Reference

Haller B. C., and P. W. Messer, 2018 SLiM 3: Forward genetic simulations beyond the Wright–Fisher model. Mol. Biol. Evol. msy228-msy228.

Henn B. M., L. R. Botigué, S. Peischl, I. Dupanloup, M. Lipatov, *et al.*, 2016 Distance from sub-Saharan Africa predicts mutational load in diverse human genomes. Proc. Natl. Acad. Sci. 113: E440--E449. https://doi.org/10.1073/pnas.1510805112

Jagoda E., D. J. Lawson, J. D. Wall, D. Lambert, C. Muller, *et al.*, 2017 Disentangling Immediate Adaptive Introgression from Selection on Standing Introgressed Variation in Humans. Mol. Biol. Evol. 35: 623–630. https://doi.org/10.1093/molbev/msx314

Marnetto D., and E. Huerta-Sánchez, 2017 Haplostrips: revealing population structure through haplotype visualization. Methods Ecol. Evol. 8: 1389–1392. https://doi.org/10.1111/2041-

Supplementary Table1: Candidate adaptive introgression regions considered in this study (5MB windows)

Coordinate (hg19)	Identifier in this study	Adaptive Introgression Gene(s)	Donor Population	Recipient population	Biological Pathway(s)	Original Report
9:14-19MB	BNC2	*BNC2*	N	Europeans	Skin pigmentation	Vernot, Akey 2014
19:32-37MB	CHR19region	*RHPN2 GPATCH1 WDR88 LRP3 SLC7A10*	N	Europeans	*multiple genes and pathways	Browning et al. 2018
3:43-48MB	CHR3region	*CCR9 LZTFL1 FYCO1 CXCR6 XCR1*	N	South Asians	*multiple genes and pathways	Browning et al. 2018
2:43-48MB	EPAS1	*EPAS1*	D	East Asians (Tibetans)	High altitude adaptation	Huerta-Sanchez et al. 2014
11:9-14MB	GALNT18	*GALNT18*	N	South Asians	Glycan biosynthesis	Browning et al. 2018
6:29-34MB	HLA	*HLA-A, HLA-B, HLA-C*	N, D	Eurasians, Oceanians	Immune system regulation	Abi-Rached et al. 2011
3:48-53MB	HYAL2	*HYAL2*	N	East Asians	Cell proliferation, metabolism	Ding et al. 2014
12:50-55MB	KRT71	*KRT71, KRT6A, KRT5*	N	Eurasians	Keratinization, ectoderm differentiation	Browning et al. 2018, Vernot, Akey 2014
16:54.5-59.5MB	NLRC5	*NLRC5*	N	East Asians	Innate immunity sensor	Descamps et al. 2016
12:111-116MB	OAS123	*OAS1, OAS2, OAS3*	N, D	Eurasians	Toll-like receptor signaling	Mendez et al. 2013, Sankararaman et al. 2014
15:25.5-30.5MB	OCA2	*OCA2*	N	Eurasians	Skin pigmentation	Gittelman et al. 2016
10:93-98MB	PDE6C	*PDE6C*	N	Eurasians	Nucleotide metabolism and	Vernot, Akey 2014

					phototransductio n	
11:117.5-122.5MB	POU2F3	*POU2F3*	N	East Asians	Keratinocyte proliferation and differentiation	Vernot, Akey 2014
12:119-124MB	RNF34	*RNF34*	N	Eurasians	Innate immune system	Vernot, Akey 2014
15:46-51MB	SEMA6D	*SEMA6D*	N	Eurasians	Semaphorin interaction	Vernot, Akey 2014
4:52-57MB	SGCB	*SGCB, SPATA18*	N	Eurasians	Cardiomyopathy, mitochondrial metabolism	Vernot, Akey 2014
8:85-90MB	SGCZ	*SGCZ*	N	South Asians	Cellular regulation	Browning et al. 2018
1:230-235MB	SIPA1L2	*SIPA1L2*	N	East Asians	Neuronal signaling	Vernot, Akey 2014
17:5.06-10.06MB	SLC16A11	*SLC16A11*	N	Native Americans	Lipid metabolism, Type 2 Diabetes	Williams et al. 2014
2:226-231MB	SLC19A3	*SLC19A3*	N	South Asians	Vitamin digestion and absorption	Browning et al. 2018
17:16.5-21.5MB	SLC5A10	*SLC5A10*	D	Europeans	Hexose transport and metabolism	Racimo et al. 2017
12:54.5-59.5MB	STAT2	*STAT2*	N	Eurasians, Oceanians	Immune system regulation	Mendez et al. 2012
1:117-122MB	TBX15	*TBX15/WAR2*	D	Native Americans	Adipose tissue differentiation	Racimo et al. 2017
4:37-42MB	TLR1610	*TLR1610*	N	Europeans	Immune system regulation	Gittelman et al. 2016, Descamps et al. 2016
6:135.5-140.5MB	TNFA1P3	*TNFA1P3*	N, D	Oceanians	Immune system regulation	Gittelman et al. 2016
9:110-115MB	TXN	*TXN*	N	East Asians	Redox reactions	Browning et al. 2018

This tables shows the adaptive introgression candidate regions identified in modern humans that are used in this study. The first column indicate the 5MB region range with format of chromosome:coordinate range (Hg19). The second column shows the identifier of the region in this study, and the third column shows the AI candidate genes included in the region. The fourth column shows the identified archaic introgression group, with N = Neanderthals and D = Denisovans. The fifth column shows the modern human populations where the AI signature are identified. The sixth column shows the biological pathways involved by the genes. The original studies reporting the AI signature are shown in the last column.

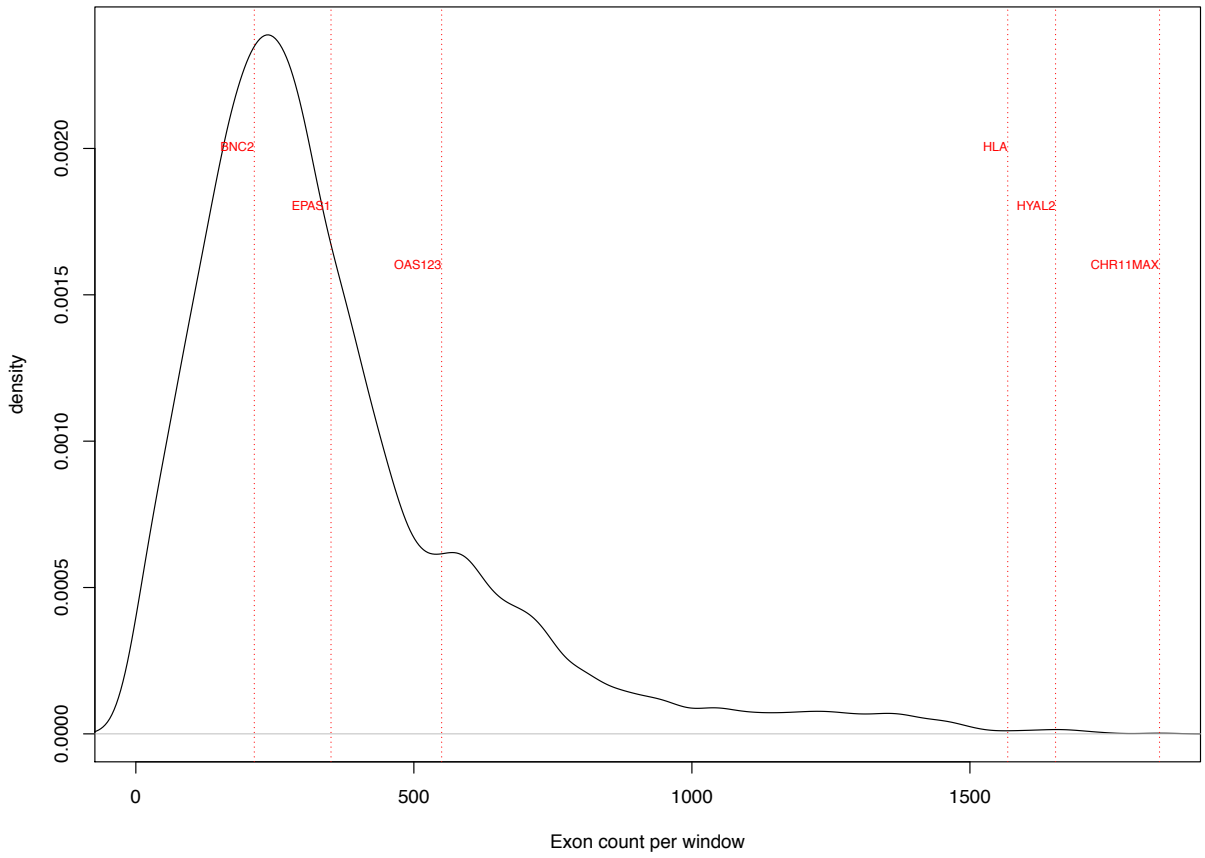

Figure S1: Exon density distribution in human genome (5MB windows)

This figure shows the exon density distribution of 5MB-windows in human genome. The exon density is defined as the number of exons within a 5MB window. The whole human genome (hg19) was scanned in 5MB sliding windows with 100kb step size, and the exon density distribution is plotted as the black solid line. Each vertical red dotted line shows the exon density of the AI candidiate regions that are mentioned in the main text (identifiers shown in Table S1).

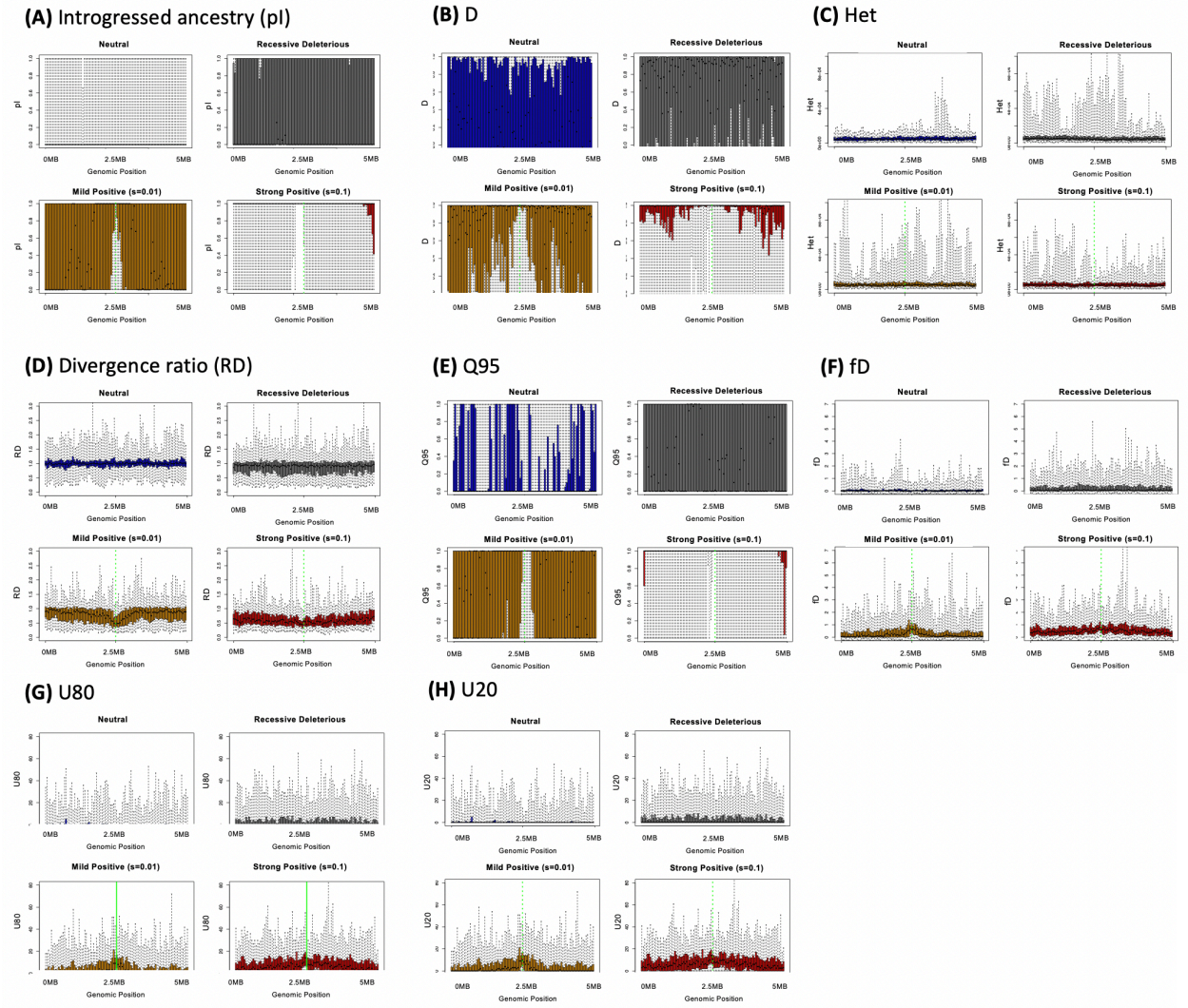

Figure S2: AI summary statistics distribution under Model_0 using uniform low recombination rates of 1e-9 (*Chr11max* region)

A-H show the distributions of AI statistics in 50kb windows across the 5MB region on Chr11. See main text Table 1 for the definitions of each statistic. For each 50kb window (the x-axis), we plot the interquartile distributions of the statistics over 200 simulation replicates in boxes, with whiskers extending to all data points. Mutations are (blue) neutral, (gray) recessive and deleterious with selection effects drawn from a gamma DFE, (orange) same as panel B with a single mildly beneficial (s=0.01) mutation, and (red) same as panel B with a single highly beneficial (s=0.1) mutation. The adaptive mutations in the latter two mutation models are introduced in window in the middle of the region (2.5MB), indicated by the green solid line. Recombination was simulated at a uniform rate of 1e-9 per site. We simulated under the demography described by Model_0 (see main text Figure 2), and obtained 200 replicates per scenario.

(A) Group and sort haplotypes based on decreasing similarity to the donor population

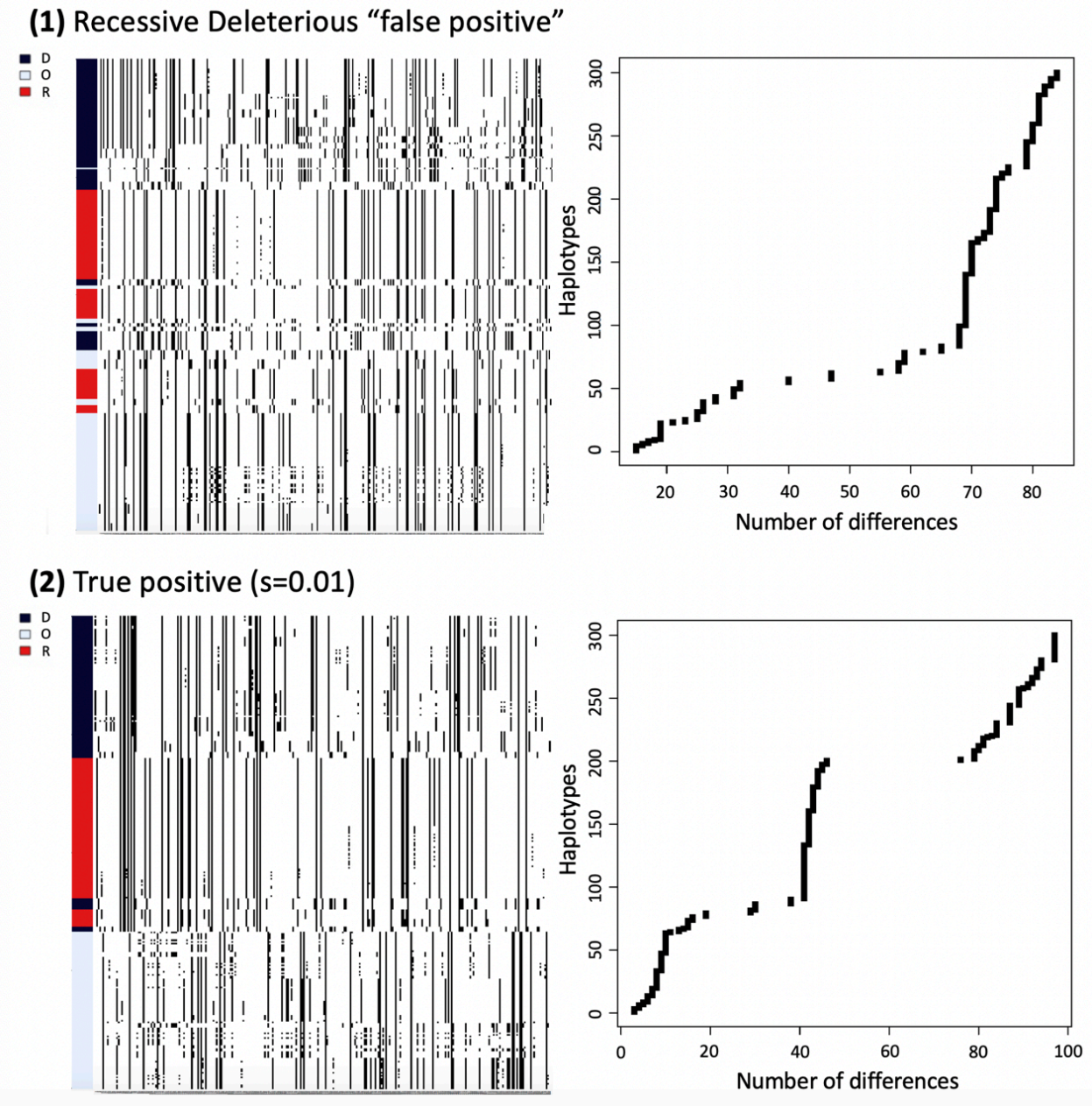

(B) Group haplotypes by populations, sorting by distance to the donor population

(1) Recessive Deleterious "false positive" (2) True Positive (s=0.01)

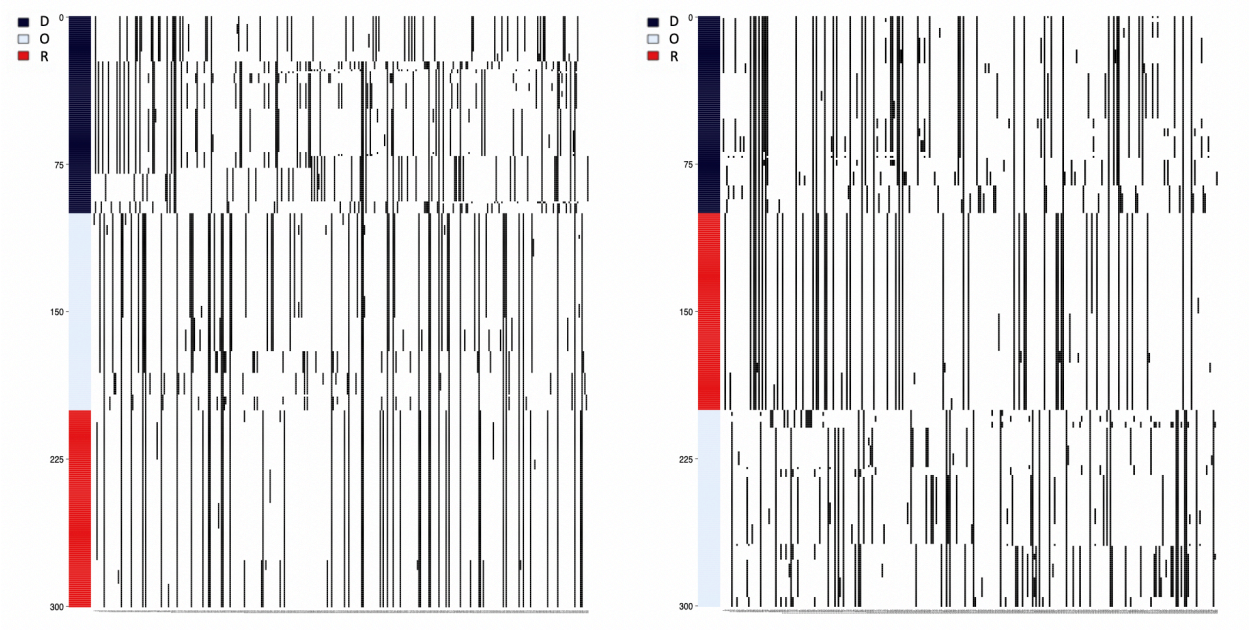

Figure S3: Haplotype patterns at 100kb window surrounding the adaptive allele

For each type of simulation, we sampled 100 haplotypes (rows in the heatmap) in the middle 100kb region of the Chr11Max segment each from the outgroup, recipient, and the donor populations (Model_0 simulations, with uniform recombination rate at 1e-9). We clustered and sorted the haplotypes by decreasing distance to the donor population haplotypes (Figure S3A), or clustered by population first before sorting by decreasing distance to the donor population (Figure S3B). The panels next to the heatmaps label haplotypes from the donor (pD, in black), recipients (pR, in red) and outgroup (pO, in light blue) populations. The right-hand side of panel A are the number of differences between the donor haplotypes and the individuals in the recipient population sorted by decreasing similarity.

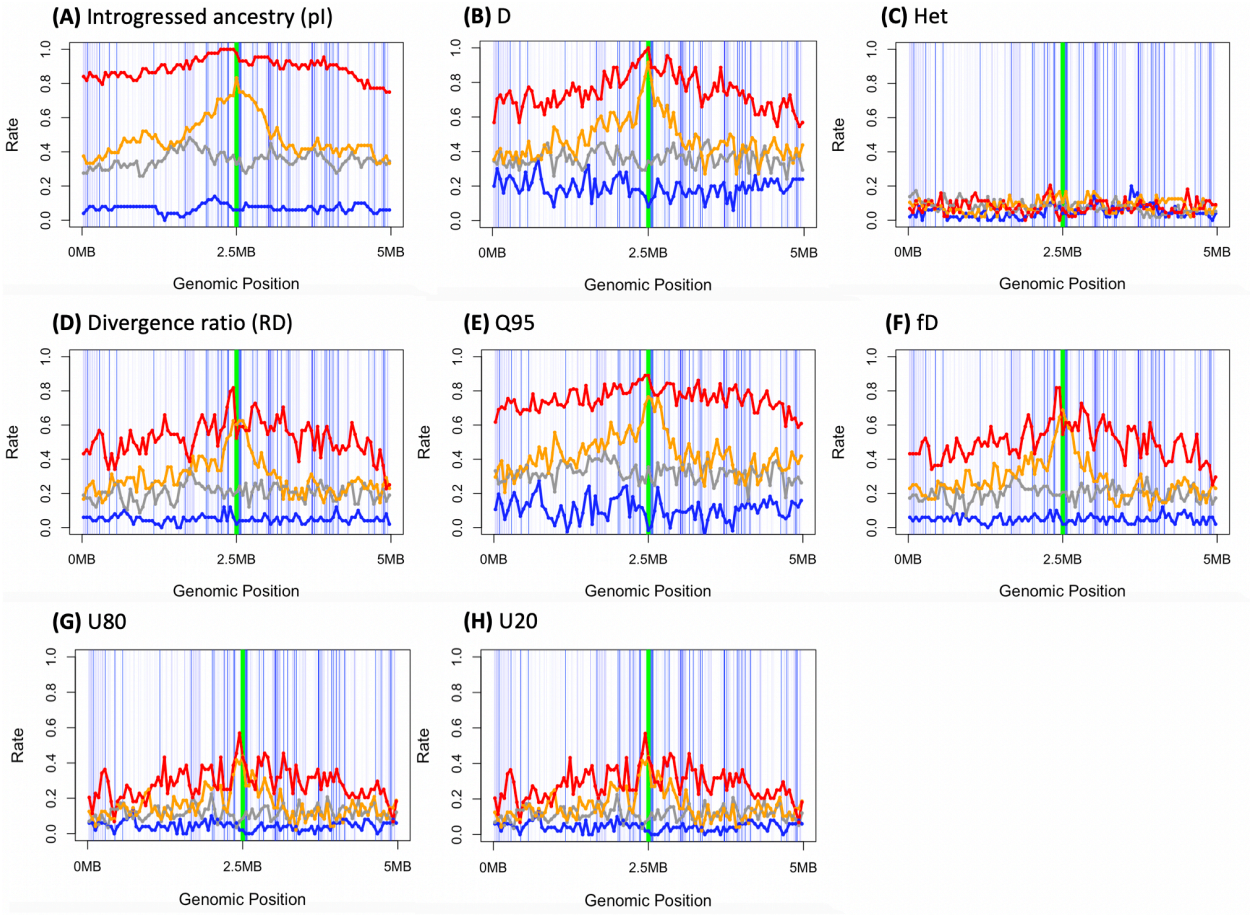

Figure S4: False positive rate distribution of AI summary statistics under Model_0 using uniform low recombination rates of 1e-9 (*Chr11max* region)

A-H show the False Positive Rates (under the neutral and deleterious models) and the True Positive Rates (under the models with positive selection) for each 50kb window using critical values defined from Figure S2 simulations. For the simulations, red, orange, blue and black represent Strong-Pos, Mild-Pos, Neutral, and Deleterious models respectively. The light blue lines illustrate the exons where new mutations can arise, and the green solid line represents the window where the adaptive mutation occurred. The simulations were run under Model_0 using the genic structure of the Chr11Max region, with a uniform low recombination rate of 1e-9.

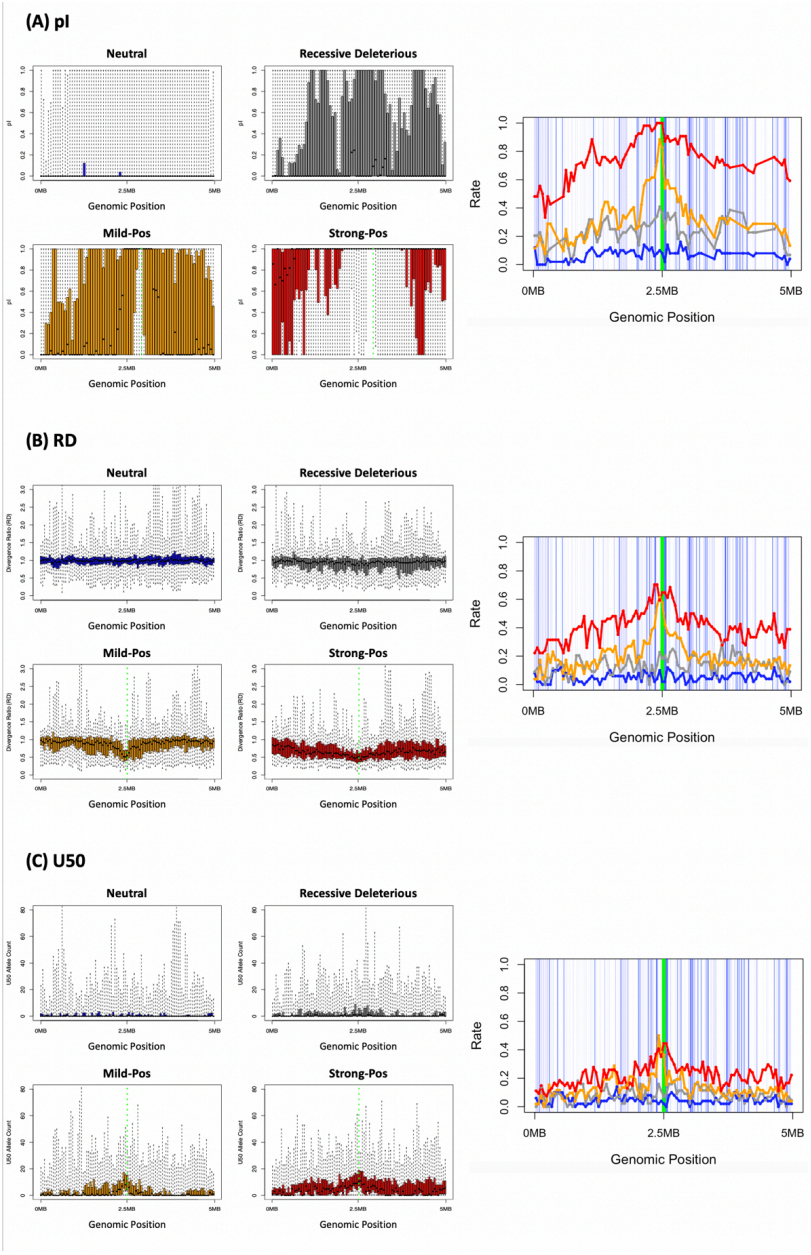

Figure S5: Distributions of pI, RD, and U50 under Model_0 using a realistic recombination rate (*Chr11max* region)

A-C show the distributions of pI, U50, and RD statistics under the four mutation models (left panels; blue for Neutral, gray for Deleterious, orange for Mild-Pos, and red for Strong-Pos), and their false/true positive rates defined using the Neutral critical values (right panels). The light blue lines illustrate the exons where new mutations can arise, and the green solid line represents the window where the adaptive mutation occurred. The simulations were run under Model_0 using the genic structure of the Chr11Max region, with a realistic recombination map for modern humans, and 200 replicates per scenario.

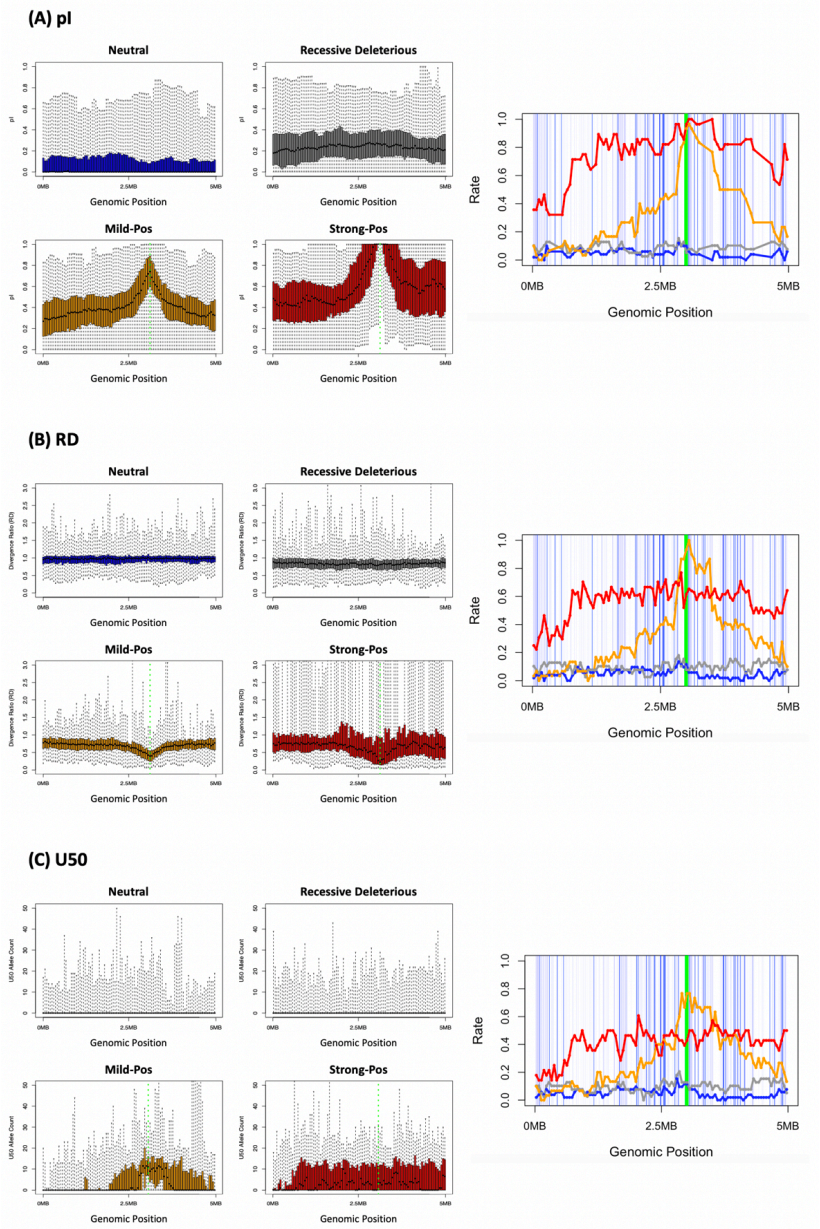

Figure S6: Distributions of pI, RD, and U50 under Model_h using realistic recombination rate (*Chr11max* region)

A-C show the distributions of pI, U50, and RD statistics under the four mutation models (left panels; blue for Neutral, gray for Deleterious, orange for Mild-Pos, and red for Strong-Pos), and their false/true positive rates defined using the Neutral critical values (right panels). The light blue lines illustrate the exons where new mutations can arise, and the green solid line represents the window where the adaptive mutation occurred. The simulations were run under the modern human demography (Model_h) using the genic structure of the Chr11Max region, with a realistic recombination map for modern humans, and 200 replicates per scenario.

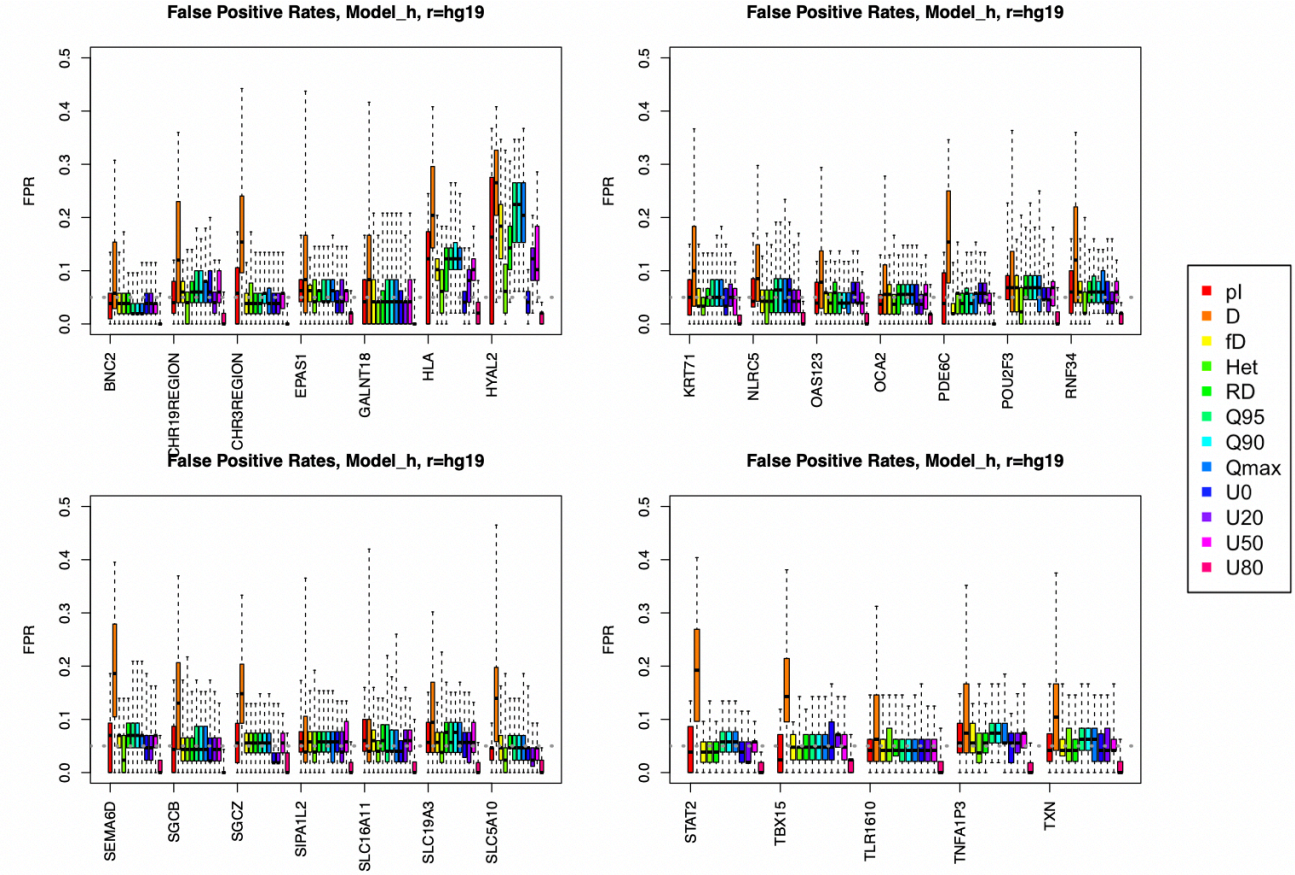

Figure S7: False positive rates (FPR) of summary statistics from human AI candidate regions under model_h using realistic recombination rates

False positive rates for several summary statistics are computed by simulating data under the Deleterious mutation model, using critical values determined from the neutral model. All simulations assume Model_h and the recombination rates and exon density of 26 AI candidate regions in modern humans (Table S1). The HLA and HYAL2-like regions result in the highest FPRs, while the other regions have constraint FPRs for most statistics except the D statistic.

(A) HYAL2

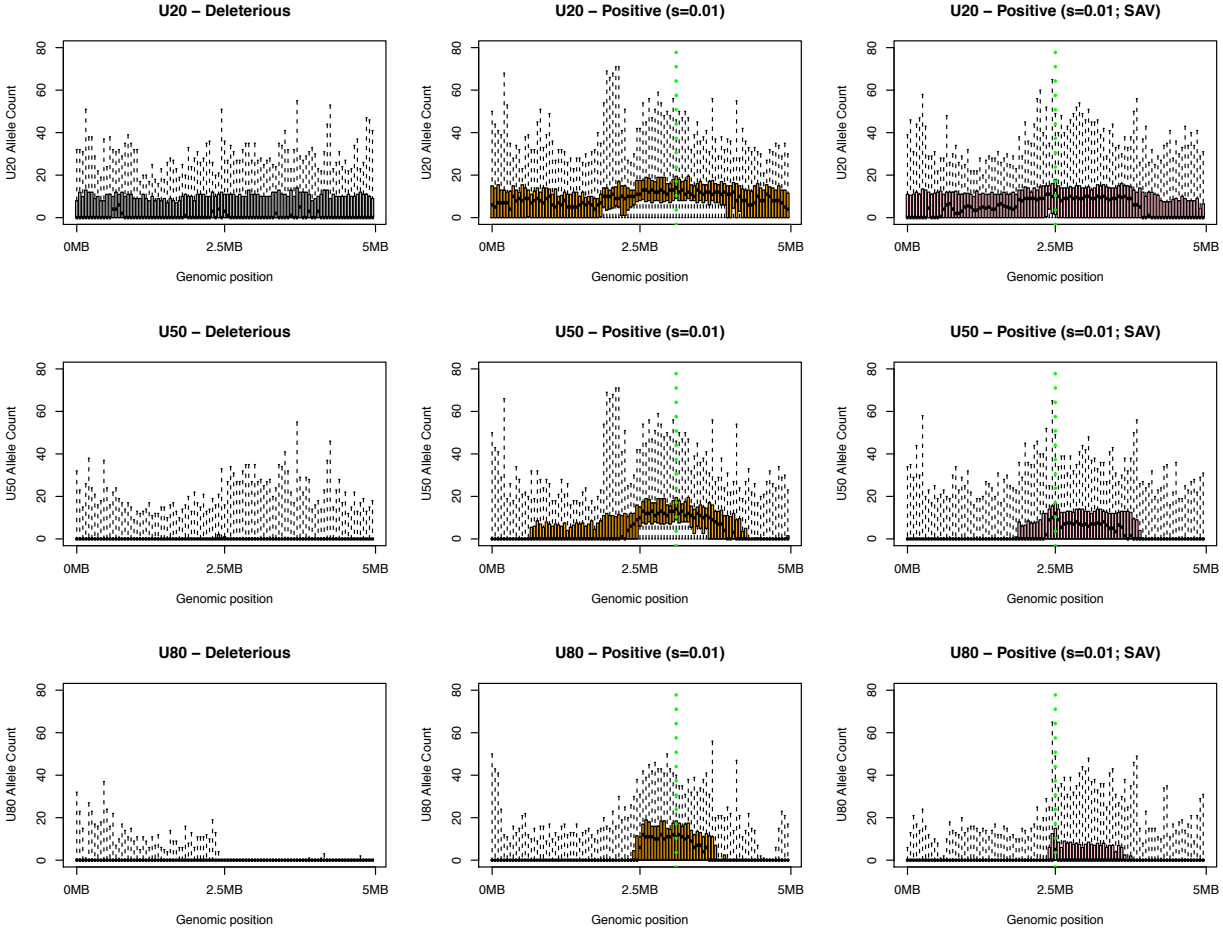
U20 – Deleterious
U20 – Positive (s=0.01)
U20 – Positive (s=0.01; SAV)
U50 – Deleterious
U50 – Positive (s=0.01)
U50 – Positive (s=0.01; SAV)
U80 – Deleterious
U80 – Positive (s=0.01)
U80 – Positive (s=0.01; SAV)
U20 Allele Count
U50 Allele Count
U80 Allele Count
0
20
40
60
80
0MB
2.5MB
5MB
Genomic position

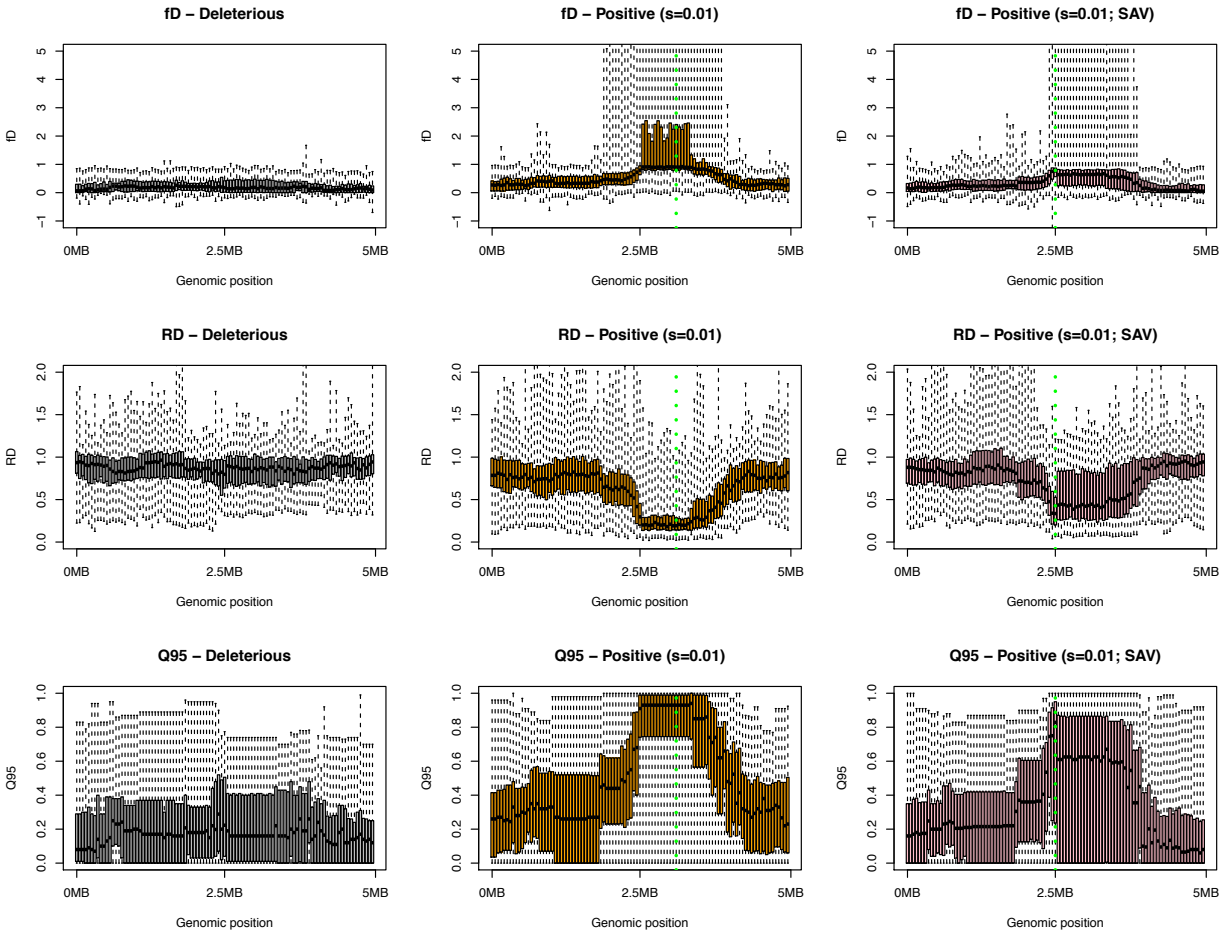
fD – Deleterious
fD – Positive (s=0.01)
fD – Positive (s=0.01; SAV)
RD – Deleterious
RD – Positive (s=0.01)
RD – Positive (s=0.01; SAV)
Q95 – Deleterious
Q95 – Positive (s=0.01)
Q95 – Positive (s=0.01; SAV)
fD
RD
Q95
0MB
2.5MB
5MB
Genomic position

(B) HLA

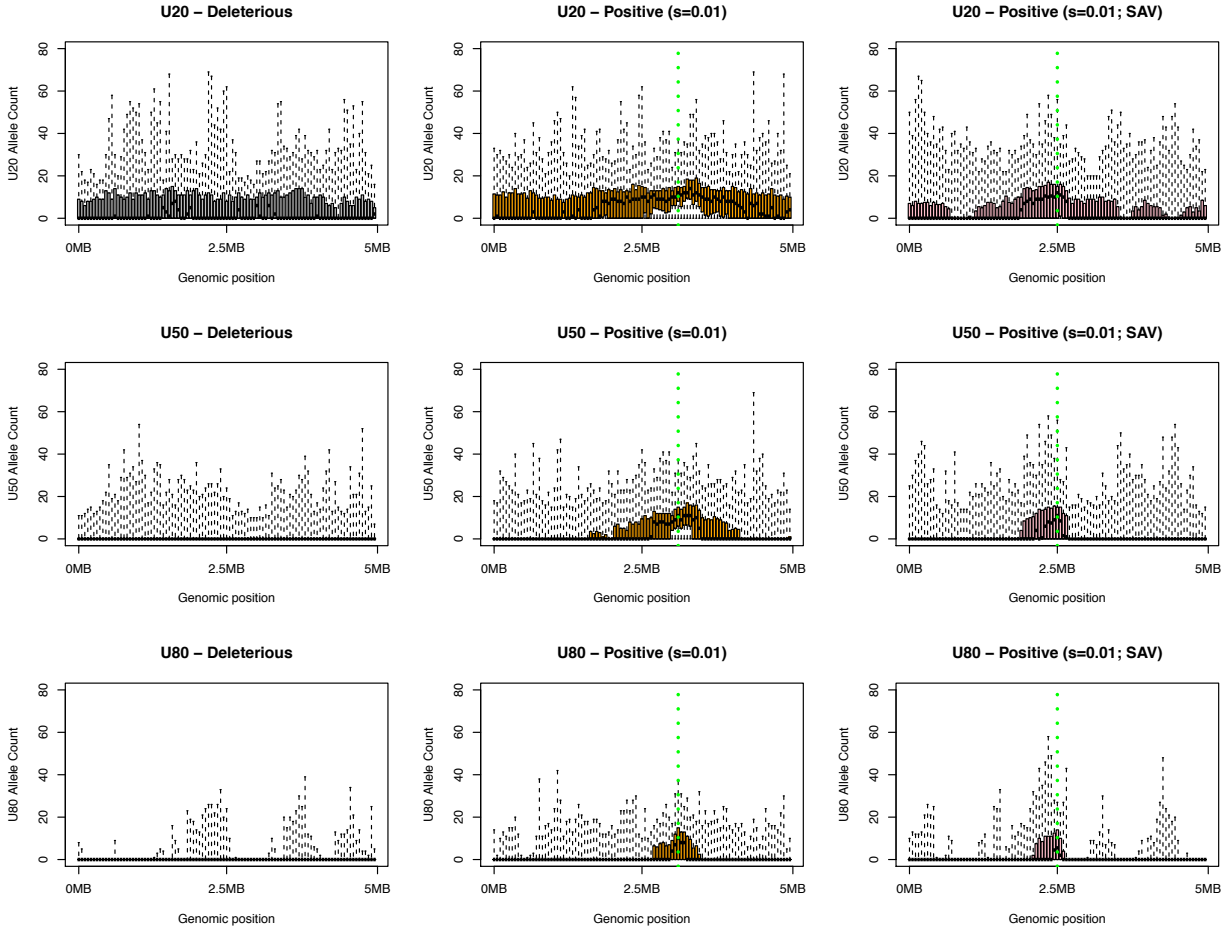
U20 – Deleterious
U20 – Positive (s=0.01)
U20 – Positive (s=0.01; SAV)
U50 – Deleterious
U50 – Positive (s=0.01)
U50 – Positive (s=0.01; SAV)
U80 – Deleterious
U80 – Positive (s=0.01)
U80 – Positive (s=0.01; SAV)
U20 Allele Count
U50 Allele Count
U80 Allele Count
0
20
40
60
80
0MB
2.5MB
5MB
Genomic position

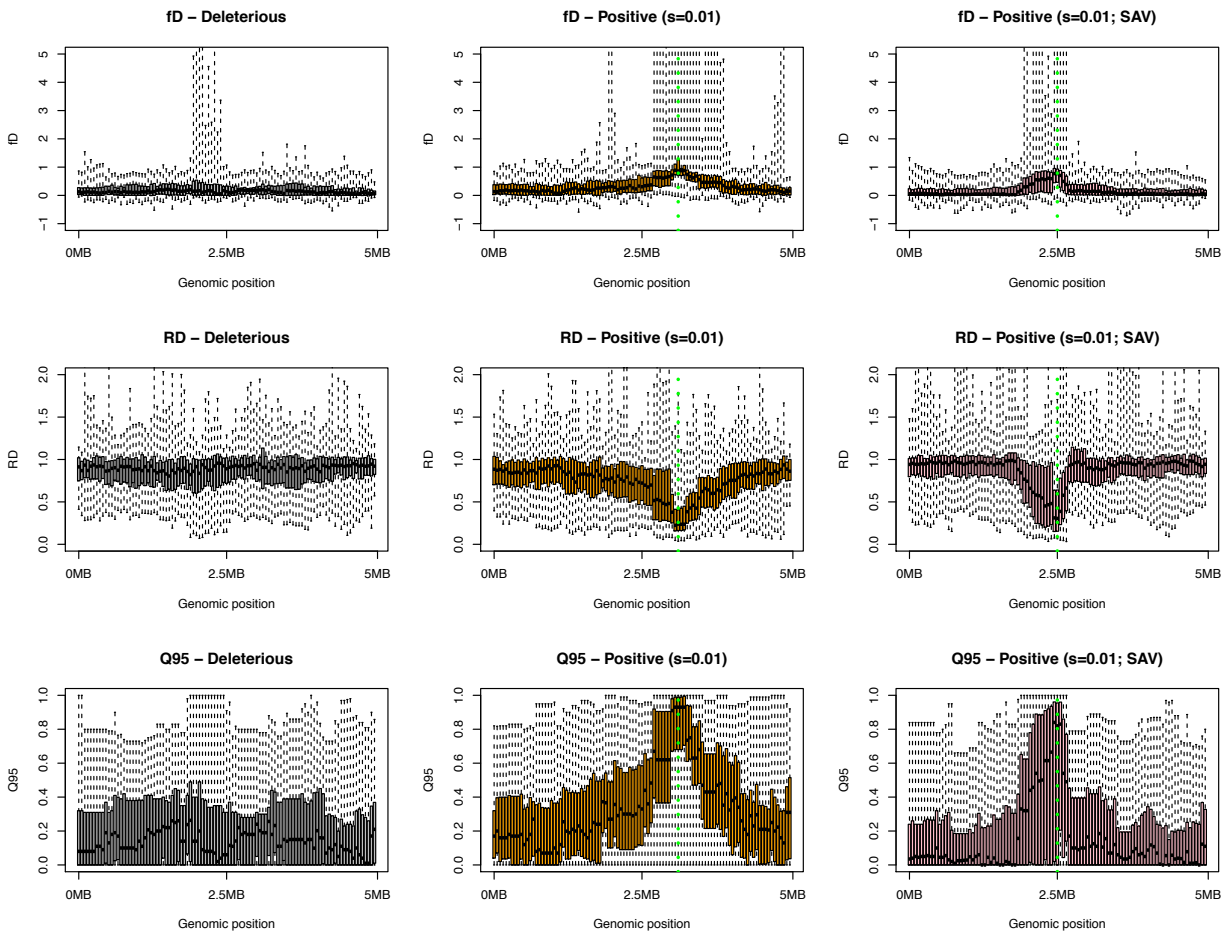

Figure S8: Comparison of the distrubitons of AI summary statistics for the recessive deleterious variants, adaptive introgression, and selection on standing archaic variation

A and B show the distributions of AI statistics in 50kb windows across the 5MB region on the HYAL2 and HLA regions, respectively. From the left to the right, the three panels each represent simulations from Deleterious (gray), Mild-Pos (orange), and the SAV model (pink) which is a variation of the Mild-Pos model except that the positive selection starts 500 generations after the introgression. The adaptive mutations in the latter two mutation models are indicated by the green solid line. Recombination was simulated using the realistic recombination map for modern humans in the two gene regions. We simulated under the demography described by modern human demography (Model_h (see main text Figure 2)) for 100 replicates per scenario.

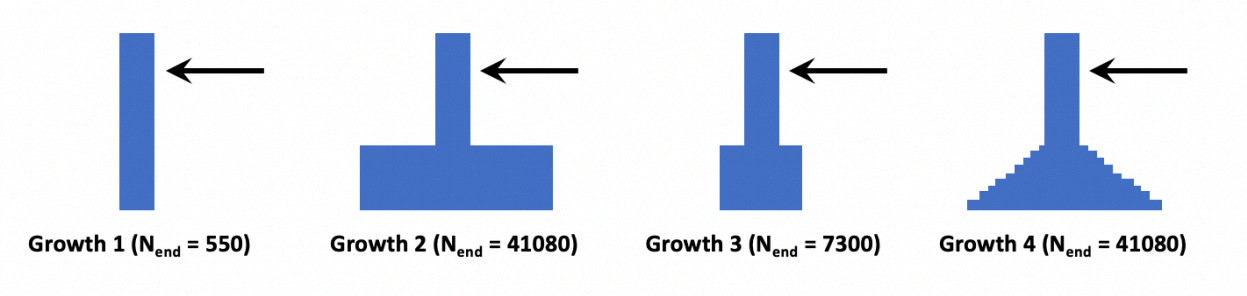

Figure S9. Four different models of population growth in recent human history

Four different demography scenarios were used to test if the recent growth in human history (Eurasian population) played a role in contributing to the false positive rates in AI detection due to the heterosis effect. "Growth 4" is the same as in Model_h (main text Fig. 2B) where the recipient population ("pR" or "Eurasian") experiences an exponential growth so that the population size at the end of the simulation (N_{end}) is 41080. As comparison, "Growth 1" experiences no population growth; "Growth 2" experiences an immediate population growth and the population stays constant after that; "Growth 3" is an intermediate situation between Growth 1 and 2 where the recipient population experiences an exponential growth but it is not as extreme as in "Growth 2". The rest of the demography remains the same as in Model_h, and the AI candidate regions are simulated under each growth pattern scenario for 200 replicates.

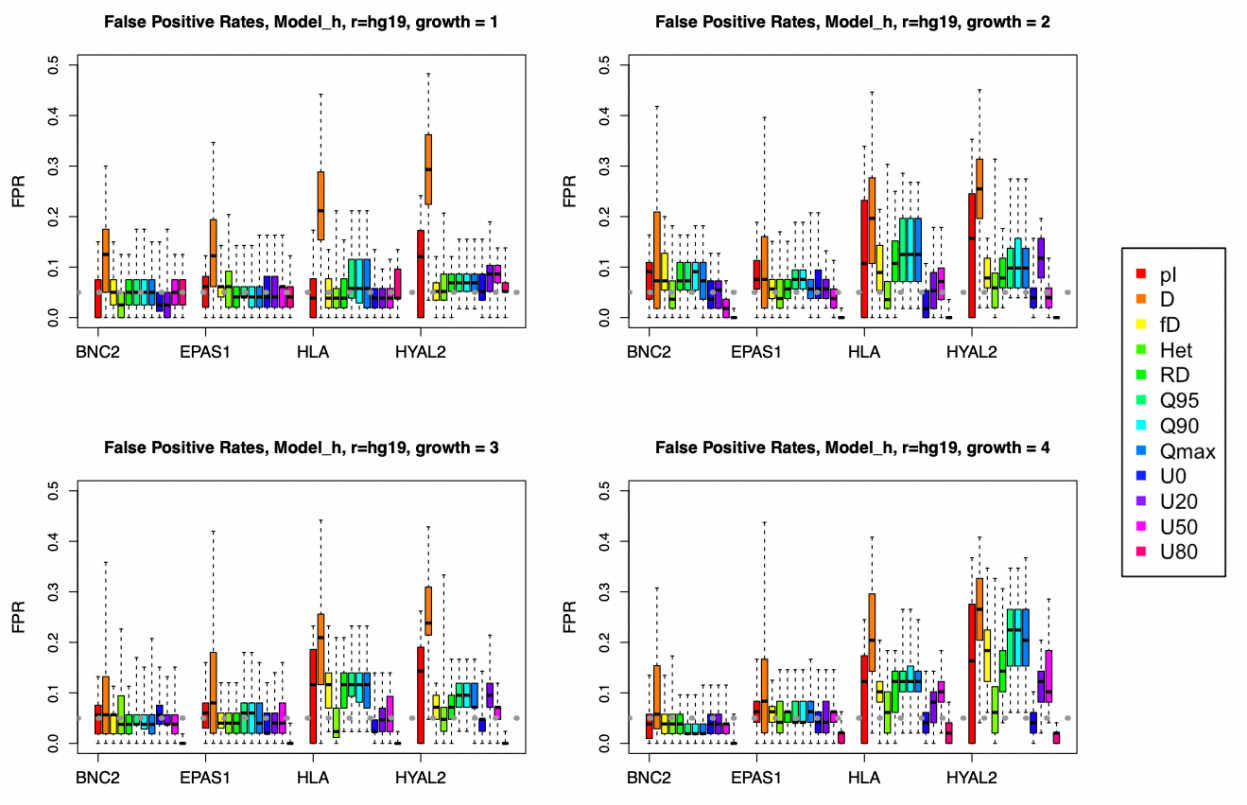

Figure S10. False Positive Rates (FPRs) under four scenarios of population growth

False positive rates for several summary statistics are computed by simulating data under the Deleterious mutation model, using critical values determined from the neutral model. The genic regions of "typical genes" (BNC2 and EPAS1) and the "outlier genes" (HYAL2 and HLA) mentioned in main text (Figure 5) are simulated. The recipient populations follows the demographic history described in Supplementary Figure S9.. In the simulations, the donor and outgroup populations assume the demography described by Model_h , and the recombination rates and exon density of the respective regions in modern humans. In general, the situations where the recipient population size at the end of the simulation is large (Growth 2 and 4) result in slightly higher FPRs especially in the outlier genes than the situations where recipient population size remain small (Growth 1 and 3). The HLA and HYAL2-like regions result in the highest FPRs in all growth pattern except in "Growth 1", where the bottleneck in the recipient population persists. The other regions have nominal FPRs for most statistics in all Growth scenarios, except for the D statistic.

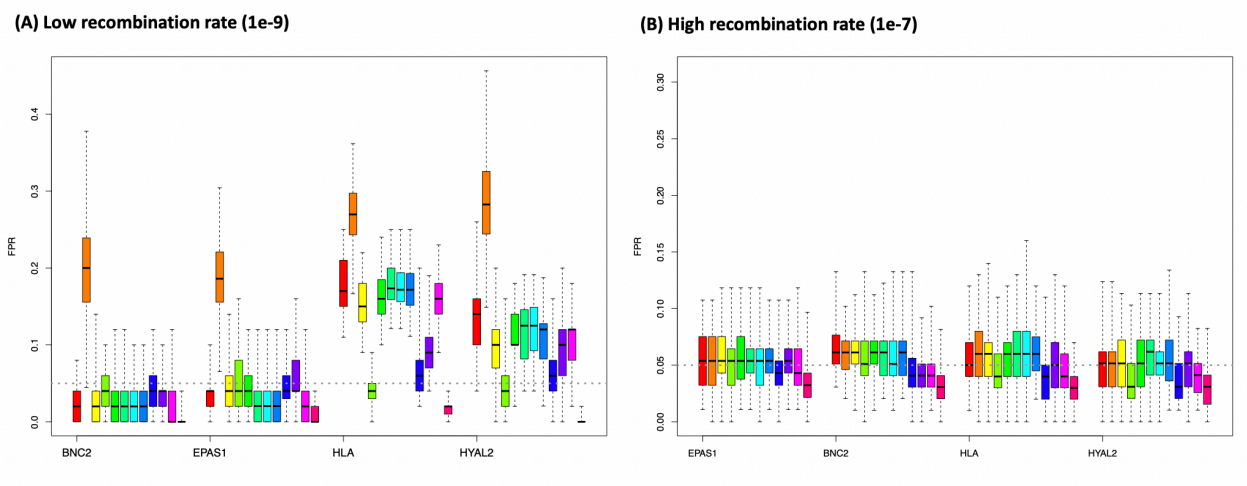

Figure S11: False Positive Rates (FPRs) under two uniform recombination rates

The genic regions of "typical genes" (BNC2 and EPAS1) and the "outlier genes" (HYAL2 and HLA) mentioned in main text Figure 5 are simulated under the Deleterious mutation model, using critical values determined from the neutral model, with each scenario repeated for 200 replicates. All simulations assume Model_h, while recombination rate is at a uniform low rate of 1e-9 (left panel), and at a uniform high rate of 1e-7 (right panel). The low recombination rate leads to higher FPRs in all regions, while they are particularly elevated for HYAL2 and HLA-like regions. Whereas, a high recombination rate controls the FPRs in all gene regions to around 5%. The color codes for the summary statistics are the same as Figure S10.

(A) HLA gene – Deleterious Model

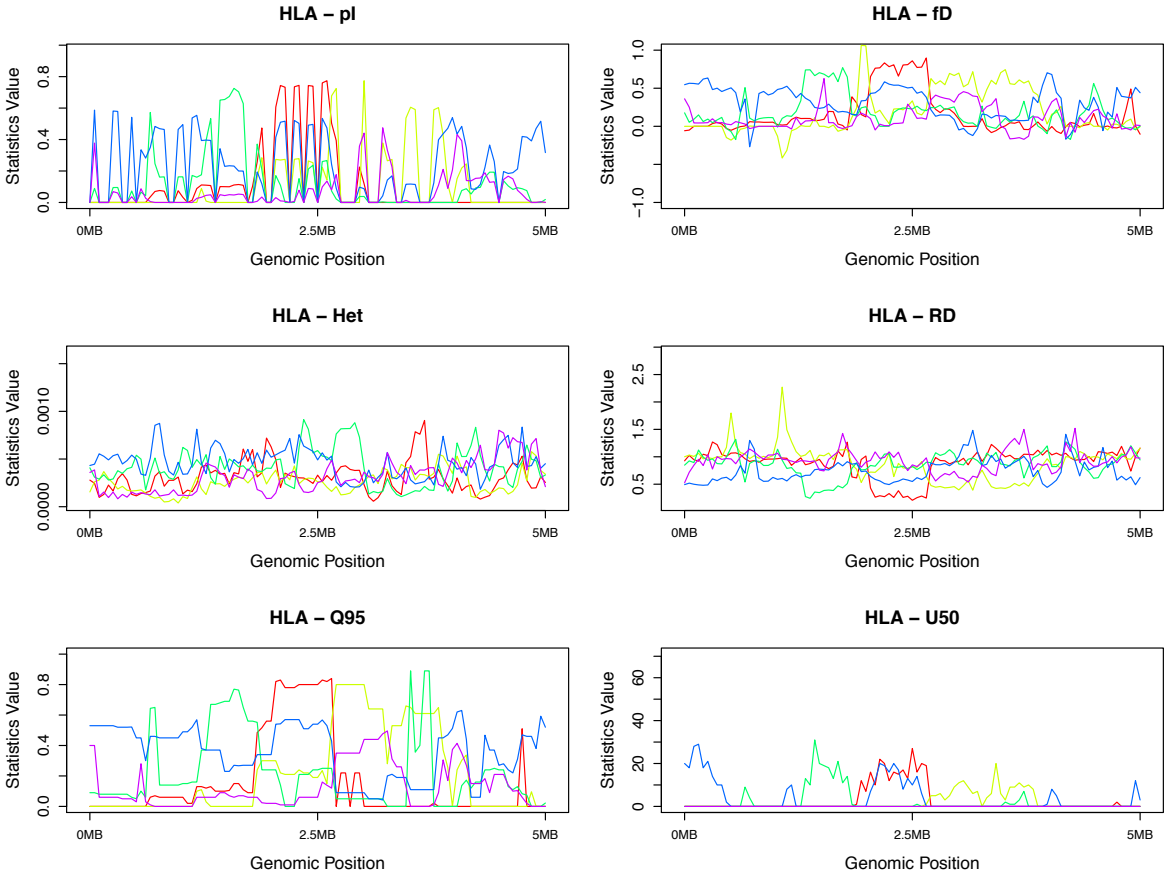

(B) HLA gene – Deleterious-Mild Model (AI)

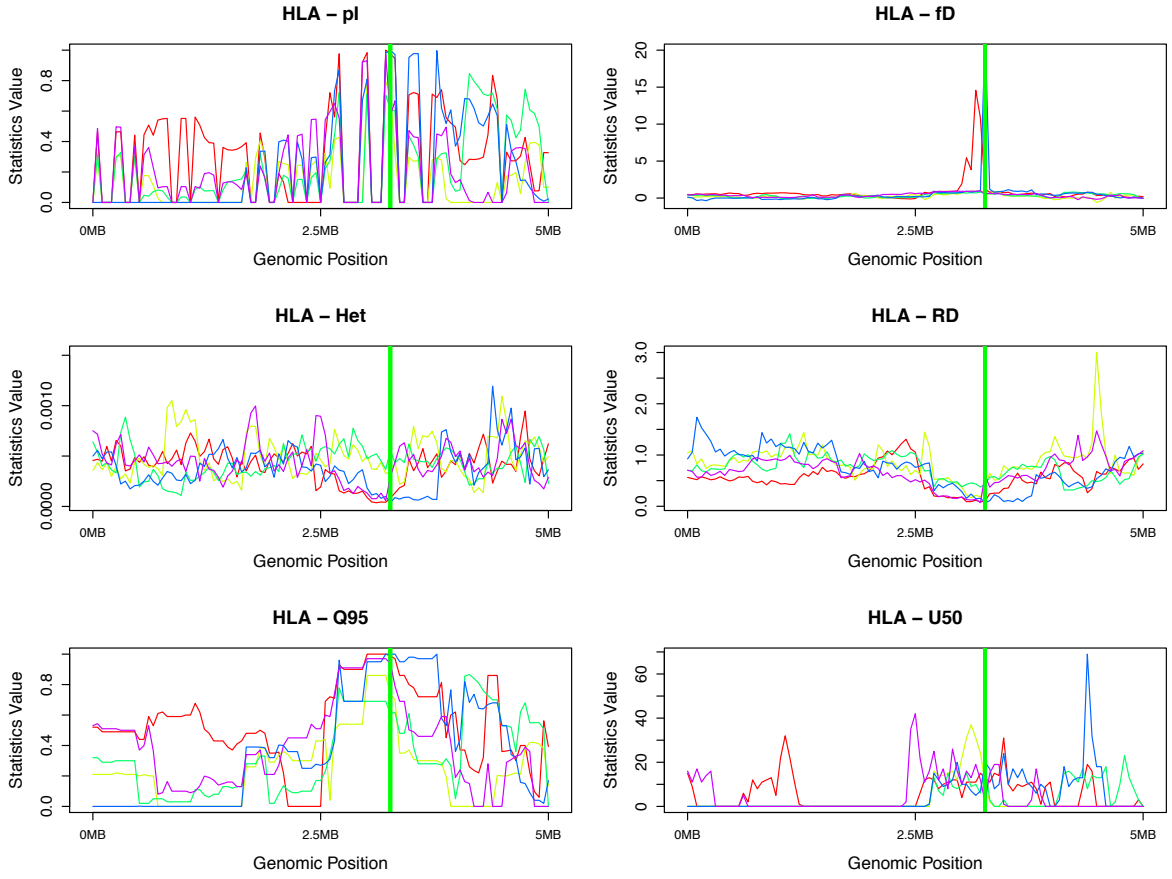

(C) HYAL2 gene – Deleterious Model

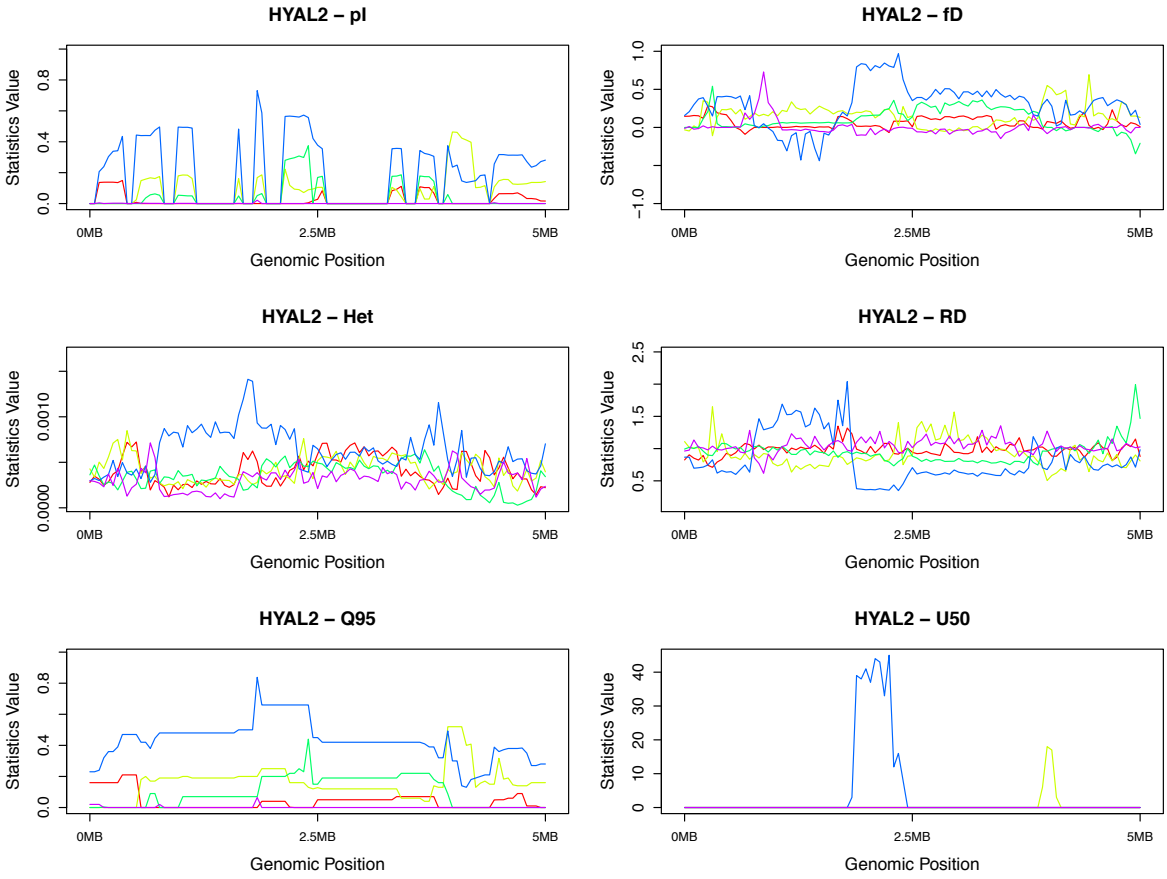

(D) HYAL2 gene – Deleterious-Mild Model (AI)

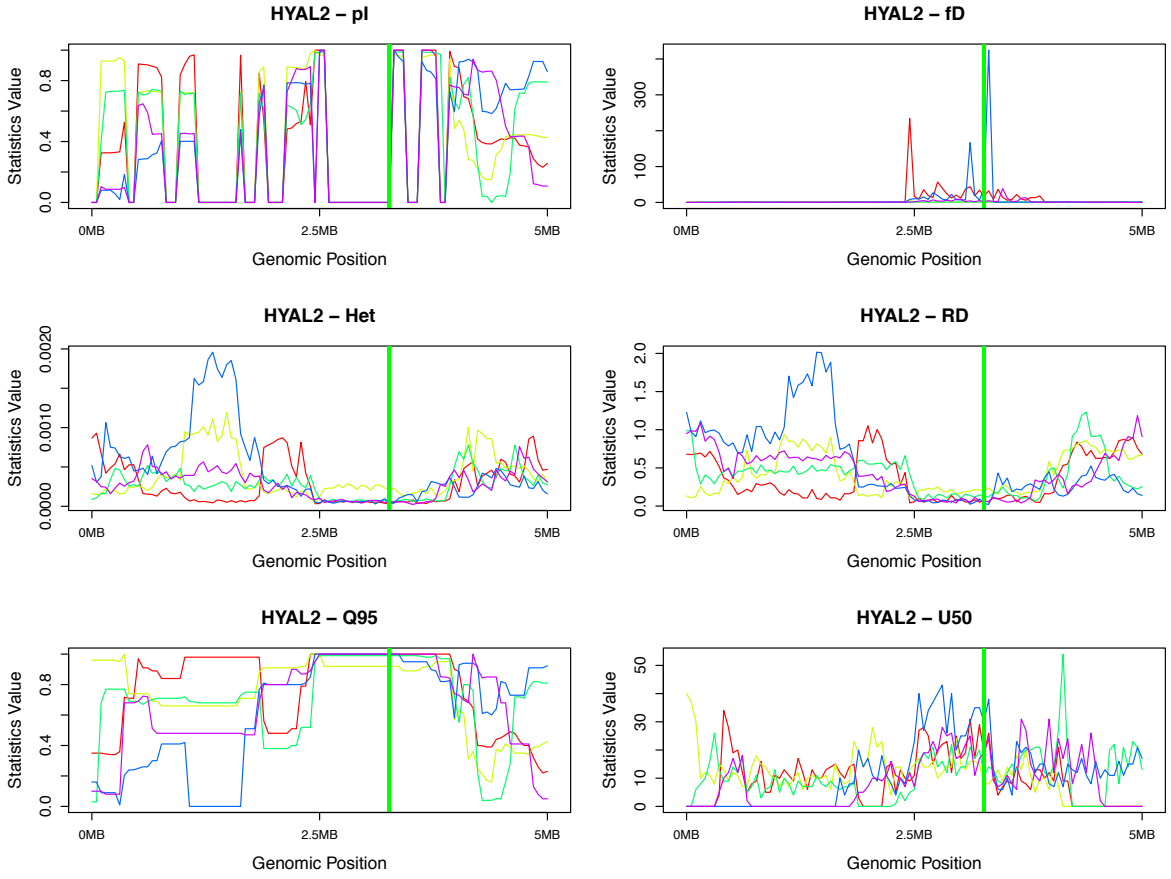

Figure S12: Distribution of summary statistics within single replicates

In the two human AI candidate genes (HLA &HYAL2) that showed high FPRs in main text Figure 5, we randomly extracted 5 single replicates from their Model_h deleterious simulations and "deleterious mild AI" simulations respectively (with realistic recombination rates). (A) HLA with deleterious mutations. (B) HLA with mild AI. (C) HYAL2 with deleterious mutations. (D) HYAL2 with mild AI. We show the distribution of six representative summary statistics values along the genomic segment, and use each unique color to represent one replicate. When there is adaptive introgression, we use a green vertical line to illustrate the location of the adaptive mutation. Here we show that the variance of statistics within each replicate is high in deleterious models, and a high peak in a given statistic is not necessarily associated with adaptive introgression.

(A) HLA gene

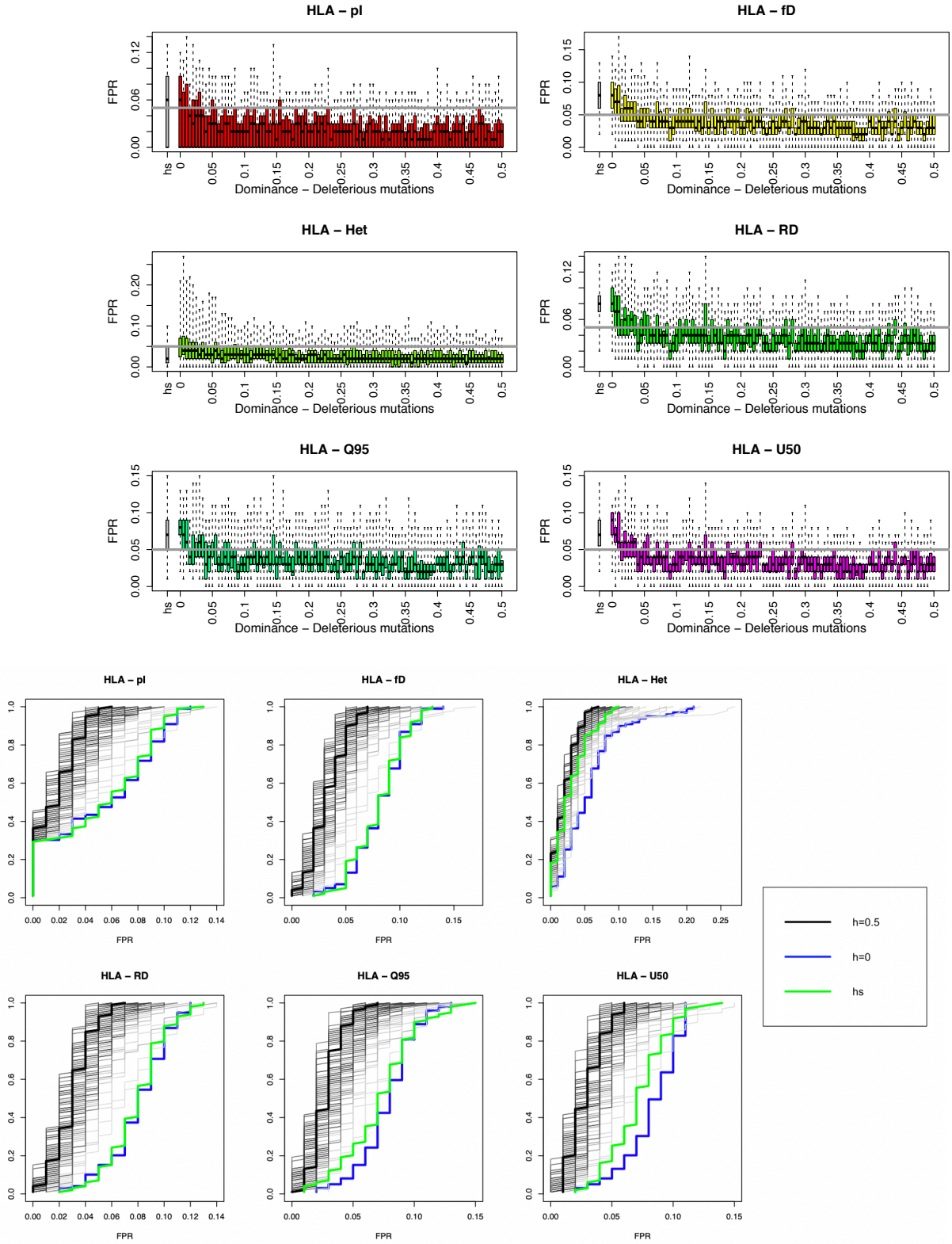
HLA – pI
HLA – fD
HLA – Het
HLA – RD
HLA – Q95
HLA – U50
FPR
Dominance – Deleterious mutations
hs
h=0.5
h=0
hs

(B) HYAL2 gene

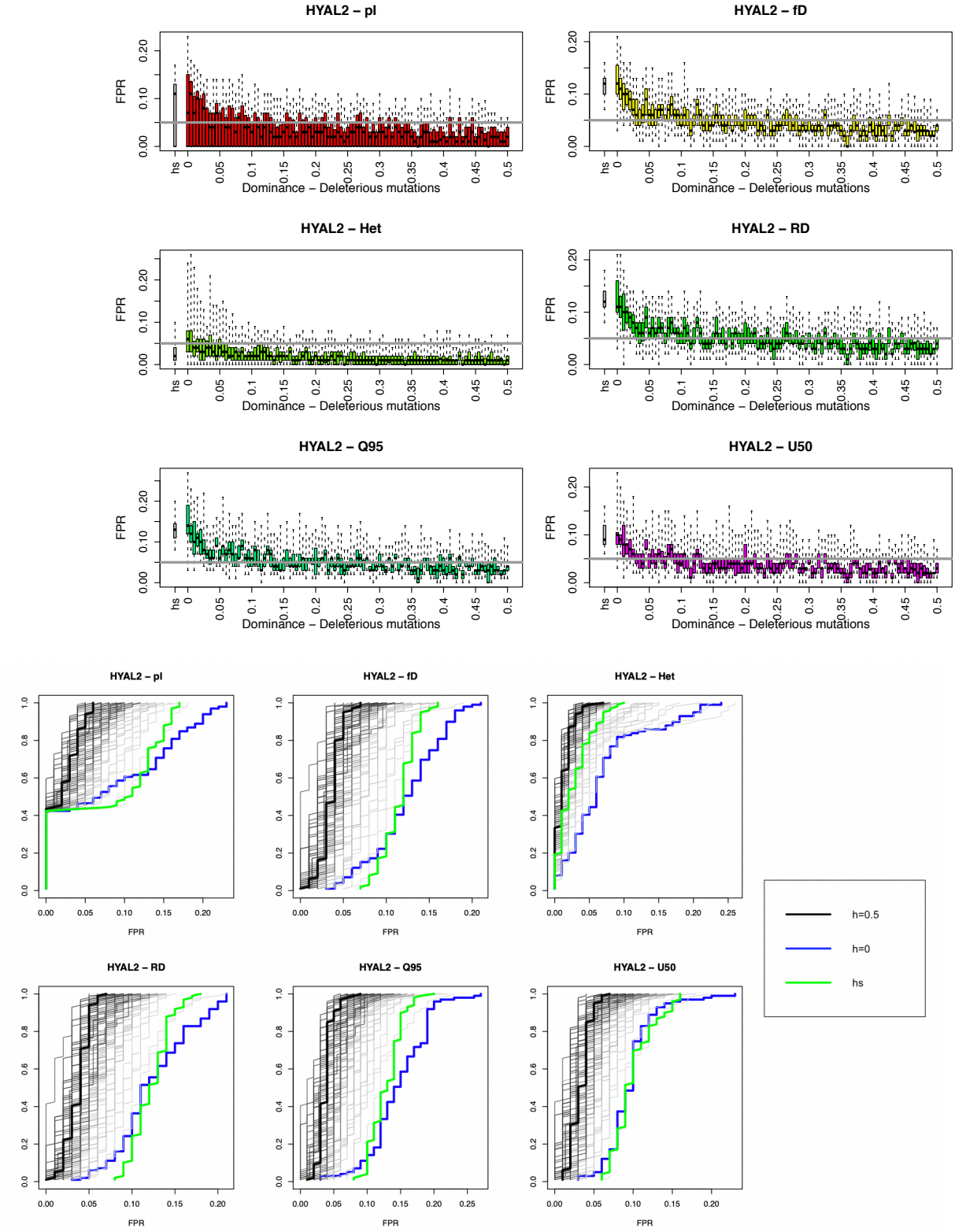
HYAL2 – pI
HYAL2 – fD
HYAL2 – Het
HYAL2 – RD
HYAL2 – Q95
HYAL2 – U50
FPR
Dominance – Deleterious mutations
hs
h=0.5
h=0
hs

Figure S13: AI summary statistics and FPRs in *HLA* and *HYAL2* genes under a range of dominance scenarios for deleterious mutations

A-B show the false positive rates on regions like the HLA and HYAL2 genes respectively in the Deleterious model, using critical values obtained from the Neutral model, and with the dominance of the deleterious mutations varying between completely recessive (h=0) and additive (h=0.5). Additionally, we show how the FPRs change when the dominance of the deleterious mutations depends on their selection strength (estimated modern human hs relationship (Henn et al. 2016); in gray bars at the left end of boxplots). The top panels show the boxplot distribution of how FPRs change with the dominance coefficient of deleterious mutations. The bottom panels show the cumulative frequency distribution of the FPRs, with black lines indicating additive, blue lines for recessive, and green lines for the hs relationship. The other h values in between the two extremes are shown in different gray lines. For the genes where high FPRs were observed under the deleterious recessive model, the FPRs remain high for most of the statistics until h approaches 0.5 (additivity). The hs relationship also shows an elevated false positive rate. All simulations shown here are performed under the Model_h demography, using a realistic recombination rate map for the respective genes, and the simulations are repeated 100 times under each dominance value.

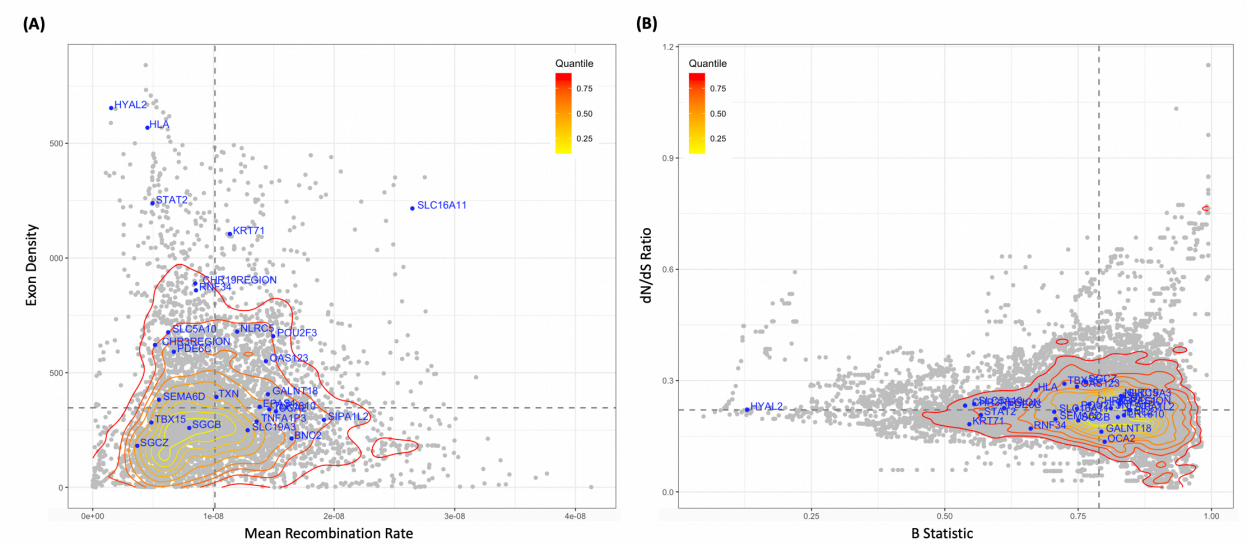

Figure S14: Genomic factors that contribute to false positive rates on the human genome

(A) The relationship between the exon density and mean recombination rate in 5MB sliding windows across the human genome (step size 100kb). (B) The relationship between background selection strength (measured by the B-statistic), and the strength of selection in protein-coding regions (measured by dN/dS ratio), on 5MB sliding windows (step size 100kb) across the human genome (hg19). A low value of B-statistic indicates stronger selection on linked variants, and a low value of dN/dS ratio indicates more constrained regions. The contour lines show the quantile of the gray points density. The blue points highlight all 26 regions of AI candidate genes mentioned in the main text). The dashed lines denote the mean values of the respective axis.

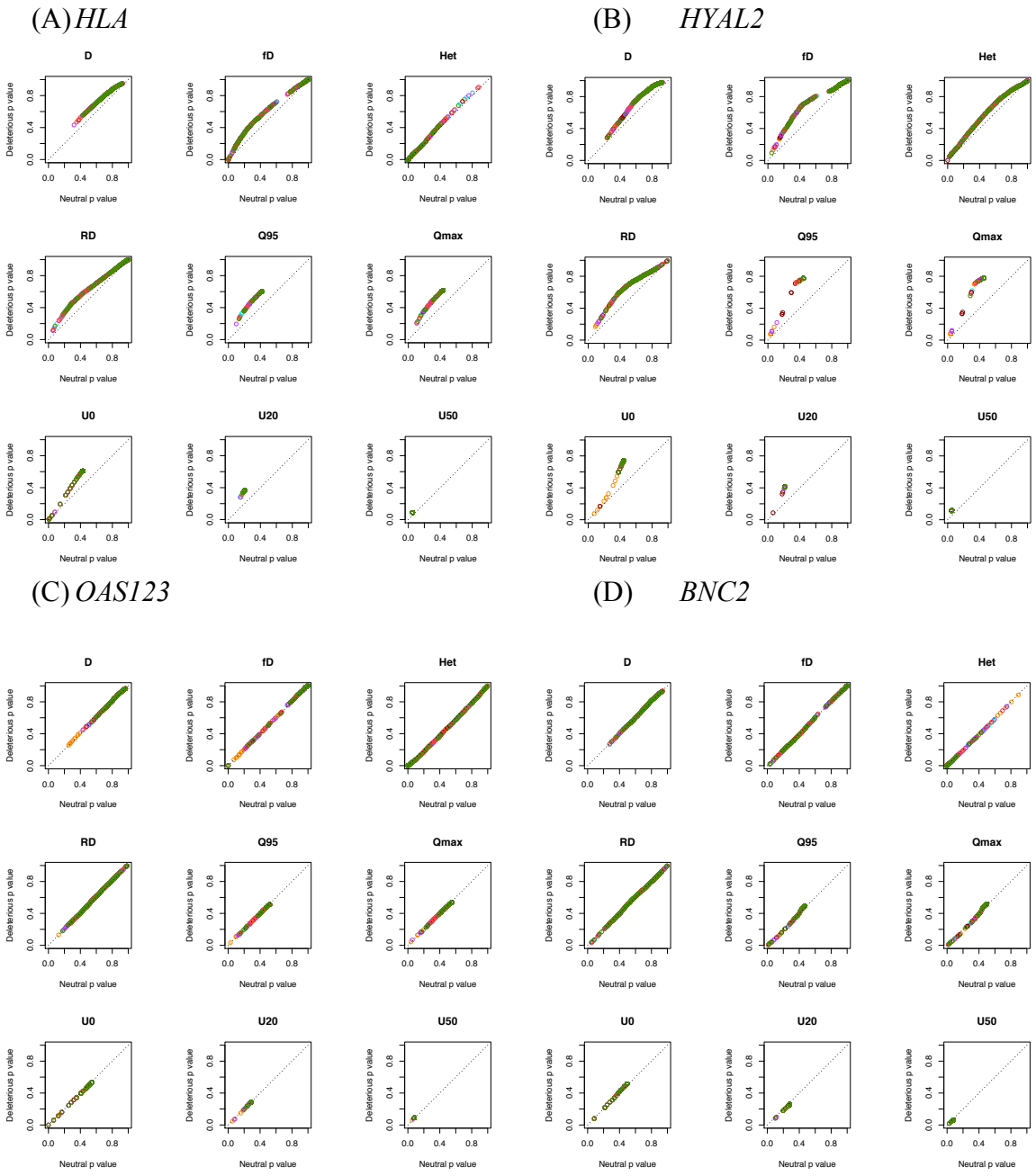

Figure S15. Comparison of *P*-values between the neutral and deleterious null models on AI candidate regions

For each 50kb-window in the empirical data, we calculated the p-value using neutral null distribution (x-axis) and deleterious null distribution (y-axis) respectively, and plotted the relationship between the two p-values as a single point. A-D denote the different genes considered. Different colors represent the 7 populations from 1000 genomes data. The points above the diagonal indicate the windows where deleterious null models made more conservative predictions in corresponding populations. Color codes for 1000 Genomes populations see main text Figure 7.

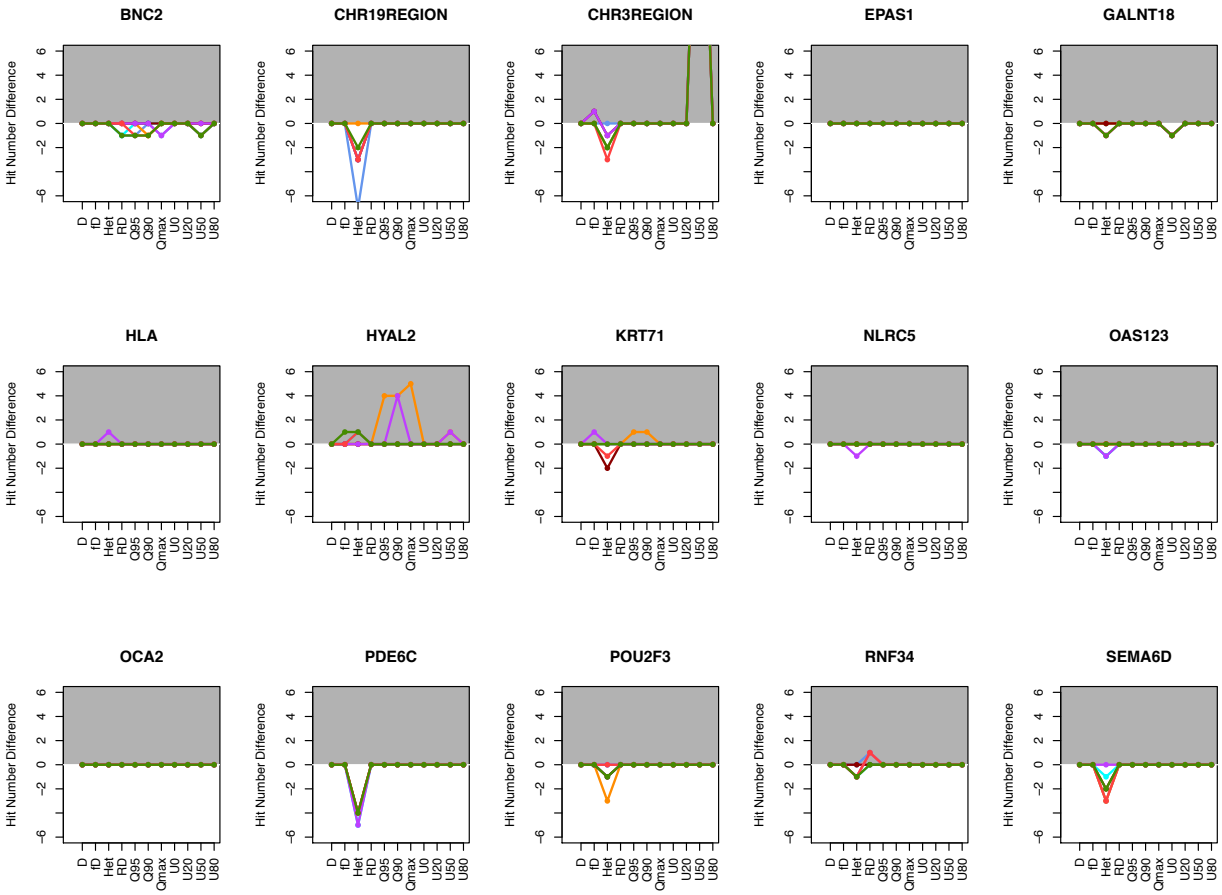
BNC2
CHR19REGION
CHR3REGION
EPAS1
GALNT18
HLA
HYAL2
KRT71
NLRC5
OAS123
OCA2
PDE6C
POU2F3
RNF34
SEMA6D
Hit Number Difference
−6
−2
0
2
4
6
D
fD
Het
RD
Q95
Q90
Qmax
U0
U20
U50
U80

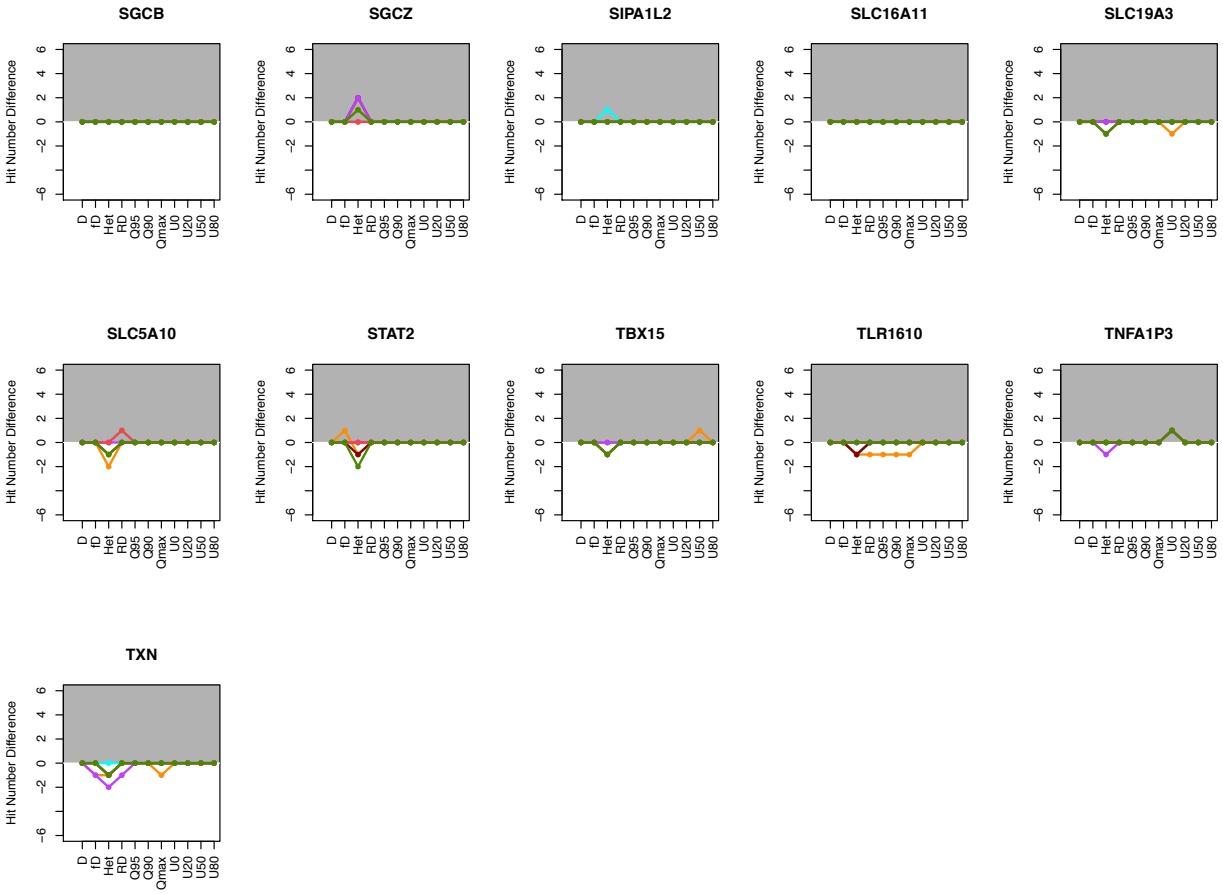

Figure S16: Differences in the number of significant windows in AI candidate regions between different null models

We compared the difference in the number of significant hits (windows with p-value <0.05) within a 500kb region that encompasses each of the 26 AI candidate genes, predicted by the neutral and the deleterious null models. Each point represents the difference in the number of hits (y-axis: Number of windows significant under a neutral model – Number of windows significant under the deleterious null model) for the statistics shown on the x-axis. The positive values, highlighted in the gray-shaded area and colored by population, imply the deleterious null model is more conservative for a given statistic. If an AI candidate region shows points above zero for most of the summary statistics, such candidate region is likely prone to false positives due to the heterosis effect, and the validity of adaptive introgression on this region requires further investigation. Color codes for 1000 Genomes populations see main text Figure 7.